J. Fluid Mech. (2024), *vol*. 993, A7, doi:10.1017/jfm.2024.594

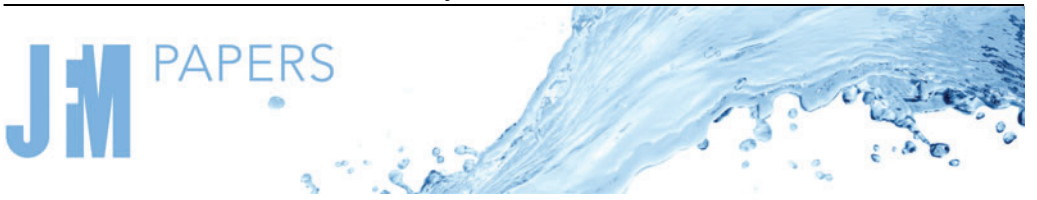

Swimming efficiently by wrapping

H. Gidituri[1], M. Ellero[1,2,3] and F. Balboa Usabiaga[1,†]

[1]BCAM – Basque Center for Applied Mathematics, Alameda de Mazarredo 14, E48009 Bilbao, Basque Country, Spain

[2]Ikerbasque, Basque Foundation for Science, Calle de Maria Diaz de Haro 3, E48013 Bilbao, Basque Country, Spain

[3]Zienkiewicz Center for Computational Engineering (ZCCE), Swansea University, Bay Campus, Swansea SA1 8EN, UK

(Received 6 March 2024; revised 10 June 2024; accepted 9 July 2024)

Single-flagellated bacteria are ubiquitous in nature. They exhibit various swimming modes using their flagella to explore complex surroundings such as soil and porous polymer networks. Some single-flagellated bacteria swim with two distinct modes, one with the flagellum extended away from its body and another with the flagellum wrapped around it. The wrapped mode has been observed when bacteria swim under tight confinements or in highly viscous polymeric melts. In this study we investigate the hydrodynamics of these two modes inside a circular pipe. We find that the wrapped mode is slower than the extended mode in bulk but more efficient under strong confinement due to a hydrodynamic increase of its flagellum translation–rotation coupling and an Archimedes' screw-like configuration that helps to move the fluid along the pipe.

Key words: micro-organism dynamics, swimming/flying, propulsion

1. Introduction

Bacteria are prokaryotic microorganisms forced to live in a zero Reynolds number environment. Due to the kinematic reversibility of viscous flows, some bacteria have developed a non-reciprocal propulsion mechanism for locomotion, the rotation of flagella. The bacterium body and the flagella are rotated in opposite directions by molecular motors. Under rotation the flagella adopt a helical shape and propel the bacterium by working as a screw. Some bacteria can move both forward or backwards, in a push or pull mode, depending on the direction of rotation of the molecular motors and on the chirality of their flagella. As bacteria are often found in confined environments they have developed different strategies to swim while foraging in those conditions. One example is a swimming mode used by some monotrichous and bipolar bacteria, where bacteria wrap

† Email address for correspondence: fbalboa@bcamath.org

their flagella around their own bodies, resembling an Archimedes' screw (Kühn *et al.* 2017; Thormann, Beta & Kühn 2022; Tian *et al.* 2022). These bacteria swim alternating between two different modes, the wrapped mode and the extended mode, where in the latter the flagella extend away from their bodies.

The wrapped mode emerges when a bacterium encounters highly viscous or strongly confined environments (Kühn *et al.* 2017). When a bacterium gets trapped during its forward pushing mode a buckling instability occurs in the flagellar hook that triggers the flagellum wrapped mode (Kühn *et al.* 2017; Park *et al.* 2022). The number of known bacterial species showcasing a wrapped mode under confinement is growing (Thormann *et al.* 2022). Thus, a natural question arises: Is the wrapped mode a mere accident or is it selected due to some advantage to the bacteria? Some studies suggest that the wrapped mode confers advantages to the motion in confinement environments. Kühn *et al.* observed experimentally that the wrapped mode can enhance the motion in highly viscous and structured environments (Kühn *et al.* 2018). Kinosita *et al.* studied the motion of bacteria with the wrapped mode in very tight confinements and concluded that the wrapped mode can allow the bacteria to glide over the substrate (Kinosita *et al.* 2018). Along this line of work we investigate how the flagellum motion in the wrapped mode favours the motion of bacteria under strong confinement by hydrodynamic interactions only. To this end we investigate the swimming of a bacterium inside circular pipes by means of computational fluid dynamics (CFD) simulations. We model the bacterium as a rigid ellipsoidal body with a single rigid flagellum attached to one of its poles, as done in previous works (Higdon 1979; Lauga *et al.* 2006). The hydrodynamic interactions between the bacterium and pipe are computed by solving the Stokes equations with the rigid multiblob method, a regularized boundary integral method (Balboa Usabiaga *et al.* 2016; Balboa Usabiaga & Delmotte 2022). We show that the extended mode is more efficient in bulk and wide pipes while the wrapped mode can be more efficient in tight pipes. The flow fields around the bacterium reveal that the wrapped mode works as an Archimedes' screw, pulling the fluid along the pipe. The scheme of the paper is the following, in § 2 we describe our numerical method and present some validations, then we describe our results in § 3 and conclude in § 4.

2. Numerical method

We model a monotrichous bacterium as a rigid ellipsoid with an helical flagellum attached to one of its poles. The flagellum is also modelled as a rigid object since it reaches an equilibrium configuration during steady-state swimming (Higdon 1979; Das & Lauga 2018). The body and the flagellum are connected by inextensible links that allow the flagellum to rotate freely around its main axis but otherwise it is forced to move concomitant to the rigid ellipsoid. Therefore, the bacterium's configuration is completely specified by seven degrees of freedom, the position and orientation of the body and the flagellum rotation, or phase angle, around its axis (Higdon 1979; Pimponi *et al.* 2016). The rigid objects, $\mathcal{B}_n$, move with linear and angular velocities, $\boldsymbol{u}_n$ and $\boldsymbol{\omega}_n$, where we use the subindex n to denote either the bacterium body or the flagellum. Due to the small bacterium size, the flow Reynolds number is vanishingly small, $Re \sim 10^{-5}$. Thus, the flow can be modelled with the Stokes equations

$$-\nabla p + \eta \nabla^2 \boldsymbol{v} = \boldsymbol{0}, \tag{2.1}$$

$$\nabla \cdot \boldsymbol{v} = 0, \tag{2.2}$$

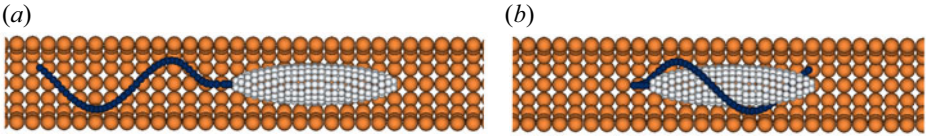

Figure 1. Bacterium, 2.04 μm long and 0.49 μm wide, inside a pipe with inner radius $r_0 = 0.4125$ μm with its flagellum in the extended and wrapped configuration. In both cases the flagellum has the same amplitude $\alpha = 0.32$ μm and the same number of waves along its axis $N_\lambda = 1.1$. Here, we show a dissected section of the pipe to make the bacterium visible.

where p and $\boldsymbol{v}$ are the fluid pressure and velocity and η its viscosity. A no-slip boundary condition is imposed on the surface of the bacterium body and its flagellum

$$\boldsymbol{v}(\boldsymbol{r}) = \boldsymbol{u}_n + \boldsymbol{\omega}_n \times (\boldsymbol{r} - \boldsymbol{q_n}) \quad \text{for } \boldsymbol{r} \text{ on the bacterium}, \tag{2.3}$$

where $\boldsymbol{q}_n$ is the tracking point of the rigid bodies (e.g. the bacterium body centre and the flagellum attachment point, respectively).

To solve the coupled fluid–structure interaction problem we use the rigid multiblob method for articulated bodies. We summarize the numerical method while a detailed description can be found elsewhere (Balboa Usabiaga & Delmotte 2022). The rigid bodies are discretized with a finite number of blobs with position $\boldsymbol{r}_i$, as shown in figure 1. As the inertia is negligible the conservation of momentum reduces to the balance of force and torque. The discrete force and torque balance for the rigid object n can be written as

$$\sum_{i\in\mathcal{B}_n} \boldsymbol{\lambda}_i - \sum_{i\in\mathcal{L}_n} \boldsymbol{\phi}_n = \boldsymbol{f}_n, \tag{2.4}$$

$$\sum_{i\in\mathcal{B}_n} (\boldsymbol{r}_i - \boldsymbol{q}_n) \times \boldsymbol{\lambda}_i - \sum_{i\in\mathcal{L}_n} (\Delta \boldsymbol{l}_{np} - \boldsymbol{q}_n) \times \boldsymbol{\phi}_n = \boldsymbol{\tau}_n, \tag{2.5}$$

where $\boldsymbol{f}_n$ and $\boldsymbol{\tau}_n$ are the external forces and torques acting on the rigid objects while $\boldsymbol{\lambda}_i$ are the constrained forces acting on the blobs that ensure the rigid motion of the bacterium body and the flagellum. The second sums in (2.4)–(2.5) run over the links, $\mathcal{L}_n$, attached to the rigid object n and $\boldsymbol{\phi}_n$ is the force exerted by the link n to keep the rigid bodies connected while $|\Delta \boldsymbol{l}_{np}|$ is the link length.

The discrete no-slip condition evaluated at each blob i is

$$\boldsymbol{v}(\boldsymbol{r}_i) = \sum_j \boldsymbol{M}_{ij} \boldsymbol{\lambda}_j = \boldsymbol{u}_n + \boldsymbol{\omega}_n \times (\boldsymbol{r}_i - \boldsymbol{q}_n) \quad \text{for } i \in \mathcal{B}_n. \tag{2.6}$$

The mobility matrix $\boldsymbol{M}_{ij}$ gives the hydrodynamic interaction between any two blobs, i and j, of radii a_i and a_j. We use a regularized version of the Oseen tensor, the Rotne–Prager tensor (Wajnryb *et al.* 2013)

$$\boldsymbol{M}_{ij} = \frac{1}{(4\pi a_i a_j)^2} \int \delta(|\boldsymbol{r}' - \boldsymbol{r}_i| - a_i) \boldsymbol{G}(\boldsymbol{r}', \boldsymbol{r}'') \delta(|\boldsymbol{r}'' - \boldsymbol{r}_j| - a_j) \, \mathrm{d}^3 r' \, \mathrm{d}^3 r'', \tag{2.7}$$

where $\boldsymbol{G}(\boldsymbol{r}, \boldsymbol{r}')$ is the Green's function of the Stokes equations and $\delta(r)$ is the Dirac delta function. The advantage of this formulation is that the regularized mobility has no divergence even when blobs get close and it is not necessary to use special quadrature rules. Equations (2.4)–(2.6) form a linear system for the unknown velocities, $\boldsymbol{u}_n$ and $\boldsymbol{\omega}_n$, and constraint forces, $\boldsymbol{\lambda}_j$ and $\boldsymbol{\phi}_n$, that can be solved efficiently with iterative methods such as the generalized minimal residual method (GMRES) (Balboa Usabiaga *et al.* 2016; Balboa Usabiaga & Delmotte 2022).

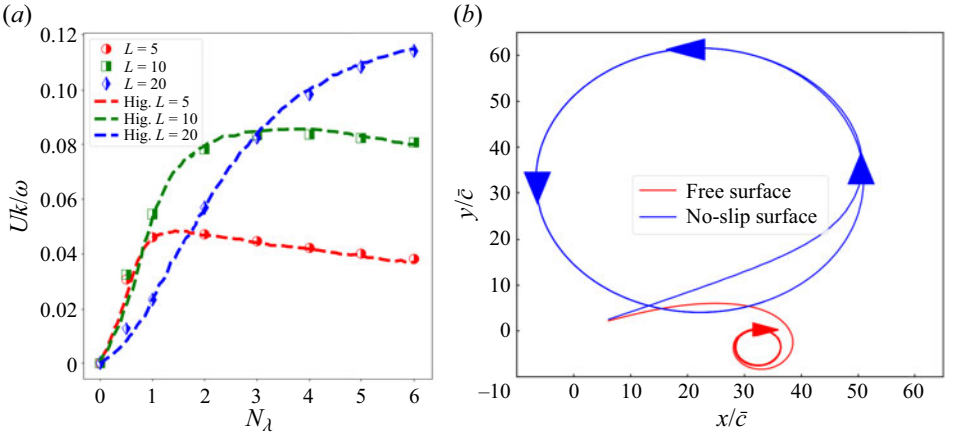

Figure 2. (*a*) Non-dimensional swimming speed, Uk/ω_{motor}, plotted against the flagellum number of waves, $N_\lambda = z_{max}/k$, for bacteria with a spherical body of radius $c = 1$ and different flagellum lengths L. The flagellum thickness, $\rho/c = 0.02$, amplitude α and wavenumber $k = 1/\alpha$ are set to compare with the results of Higdon (1979). Dashed lines represent Higdon's results while symbols represent our simulation results. (*b*) Circular trajectory comparison between a bacterium swimming above a no-slip surface and a free surface. The arrows on the curves represent the direction of swimming.

2.1. *Validation*

Here, we test our computational model against previous theoretical and computational works on helical flagellar swimming. As first validation, we compute the swimming speed, in bulk, of a bacterium formed by a spherical body of radius $c = 1$ and an helical flagellum of length L and compare our results against those of Higdon (1979). Following Higdon, we use flagella of helical shape with wavenumber k, amplitude $\alpha = 1/k$ and thickness radius $\rho/c = 0.02$. We discretize the bacterium body with 162 blobs and the flagella with 125, 250 and 500 blobs for the flagellum lengths, $L = 5$, 10, 20, respectively. We present in figure 2(*a*) the dimensionless velocity, Uk/ω, where ω is the relative angular velocity between the bacterium body and flagellum vs the number of waves in the flagellum, N_λ. The agreement with the results of Higdon is good for all the flagella considered.

As a second validation we compute the trajectory of a bacterium above a no-slip and a free-slip surface. The equations of motion are integrated with a midpoint scheme which requires solving two mobility problems per time step to find the bacterium body and flagellum velocities (Balboa Usabiaga & Delmotte 2022). The bacterium body is modelled as an ellipsoid with major axis length 4 and aspect ratio $\gamma = 2$, discretized with 287 blobs. The flagellum of length $L = 11.91$ and $N_\lambda = 2$ is discretized with 154 blobs. We also incorporate a short-range steric repulsion between the blobs and the surface to avoid possible overlaps. We use a steric repulsion of strength $f = 0.01$ pN for overlapping blobs with the surface and with an exponential decay with a characteristic length $\xi = 0.01$ μm for non-overlapping blobs. It is well known from previous studies that flagellated bacteria move in circular trajectories, of opposite directions, when swimming close to a no-slip or a free-slip surface (Lauga *et al.* 2006; Shum, Gaffney & Smith 2010; Pimponi *et al.* 2016). In addition, Pimponi *et al.* (2016) reported that the radius of the trajectory is small in the free-slip case in comparison with the no-slip case. Our results capture the previously observed features, the bacterium is hydrodynamically attracted to the surface and swims in circles, see figure 2(*b*).

Model	L (μm)	α (μm)	k (μm^{-1})	L_z (μm)	N_λ	a (μm)	N_b
I	3.29	0.32	2.27	2.57	0.8	0.0425	40
II	3.68	0.32	3.13	2.40	1.1	0.0425	43
III	4.27	0.32	4.25	2.57	1.5	0.0425	52
IV	5.11	0.32	5.66	2.57	2.0	0.0425	60
V	6.00	0.32	7.06	2.57	2.5	0.0425	72
VI	5.17	0.32	2.83	3.84	2.83	0.0425	69

Table 1. Flagellum model parameters. Flagellum length, L, amplitude, α, wavenumber, k, maximum extension along its axis, L_z, number of waves along its axis, $N_\lambda = L_z/\lambda = L_z k/(2\pi)$, blob radius, a, and number of blobs N_b. The amplitude of the wave was exponentially damped near the attachment point with a damping factor $k_E = k$, as in Higdon (1979).

Model	L (μm)	r_0 (μm)	N_b	Model	L (μm)	r_0 (μm)	N_b
I	9.35	0.4125	720	VI	14.1	0.65	1562
II	10.1	0.45	816	VII	15.1	0.7	1824
III	11.1	0.50	1008	VIII	20.1	0.95	3232
IV	12.1	0.55	1159	IX	30.1	1.45	7248
V	13.1	0.60	1386				

Table 2. Pipe model dimensions. Length L, inner radius r_0 and number of blobs N_b. The blob radius is $a = 0.1$ μm in all cases.

3. Results and discussion

In this section we study the swimming of a bacterium inside circular pipes of radius r_0 and length $L_0 \approx 21 r_0$ aligned along z. Keeping the aspect ratio constant ensures that the flow disturbance created by the bacterium decays to negligible values at the pipes ends (Liron & Shahar 1978). We model the pipes as immobile rigid objects discretized with blobs just like the bacterium (Balboa Usabiaga *et al.* 2016). We place the bacterium in the middle of the pipes and we use that configuration to compute the bacterium velocity. Since the Stokes equations assume steady-state flows, the velocity in a given configuration can be obtained by solving the mobility problem one single time. Later, we will consider the case where the bacterium freely swims inside a periodic pipe.

We consider two different swimming modes. First, the extended mode where the flagellum is attached to the body front part and it extends away from it. In the second mode the flagellum is wrapped around the bacterium body, see figure 1. In both cases we apply constant and opposite torques, of magnitude $\tau_m = 0.46$ pN μm, to the body and the flagellum to model the work exerted by a molecular motor. Thus, we assume that the molecular motor always works in the constant torque (low frequency) regime (Xing *et al.* 2006). In most numerical experiments the flagellum extends along its main axis a length similar to the bacterium body. Thus, in the wrapped mode, the body is fully covered by the flagellum. The bacterium body, always 2.04μm long and 0.49 μm wide, is discretized with 292 blobs of radius $a = 0.0425$ μm. The geometric details of the helical flagella and pipes used in this work are presented in tables 1 and 2.

All the motion is driven by the rotation of the flagellum. Therefore, we start looking at its angular velocity, ω_z, see figure 3(*a*). In bulk the flagellum rotates two times faster in the extended mode than in the wrapped mode. The slower rotation can be explained by

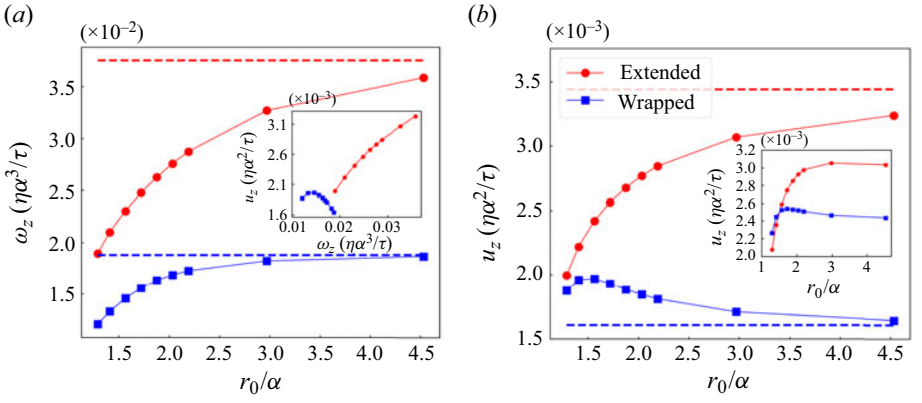

Figure 3. Flagellum angular velocity, ω_z, (*a*) and bacterium swimming speed along the pipe, u_z, (*b*) vs pipe radius r_0. Results for the extended and wrapped mode using the same flagellum (model II) with length $L = 3.6$ μm and amplitude $\alpha = 0.32$μm. The dashed lines depict bulk values. The inset in (*a*) shows the swimming speed against the flagellum angular frequency for all of the pipe radii used. The inset in (*b*) shows the swimming speed calculated with a minimal model, (3.2).

the additional drag experienced by the flagellum in the wrapped mode, which is caused by the proximity of the flagellum to the bacterium body. Both modes reduce their angular velocities as r_0 decreases due to the additional hydrodynamic drag generated by the pipe walls. However, the decrease is proportionally less important in the wrapped mode as its initial drag was larger. Thus, the ratio between the angular frequencies of the two modes falls from a factor ∼2 in bulk to a factor ∼1.6 in the smallest pipe considered.

Next, we look at the swimming speed along the pipe axis, u_z, see figure 3(*b*). We observe that in bulk the wrapped mode swims approximately twice slower than in the extended mode. This result is consistent with experimental observations (Kühn *et al.* 2017; Grognot & Taute 2021; Thormann *et al.* 2022; Tian *et al.* 2022). The slower swimming speed in the wrapped mode is a consequence of the slower rotation of its flagellum. Under confinement the swimming speed, u_z, decreases for the extended mode as the pipe radius is decreased. Again, the additional hydrodynamic drag generated by the pipe walls is responsible for this effect. In contrast, the wrapped mode exhibits a non-monotonic trend in its swimming speed. As the pipe radius is decreased the bacterium swims faster, up to the point where the ratio between the pipe radius and the flagellum amplitude is $r_0/\alpha \approx 1.5$. Beyond that point the swimming speed decreases with r_0. The striking difference between both swimmer modes is also shown in the inset of figure 3(*a*), which shows the swimming velocity vs the flagellum angular velocity for all pipe radii. Because the Stokes equations are linear the linear and angular velocity are proportional when keeping all geometric parameters constant. However, changing the pipe radius affects the proportionality constant dramatically for the wrapped mode and only weakly for the extended mode. A resolution study shows that these results are maintained after increasing the resolution of our discretization by factors 4 and 16, see the Appendix and figure 10.

We seek a physical mechanism that explains the difference between swimming modes and the speed enhancement in the wrapped case. We start by considering the motion of a single helical flagellum inside a pipe. We apply a constant torque on the helical flagellum and measure its translational and rotational speeds. Note that, in this case, the flagellum is not a torque-free swimmer, as there is no body to which to apply an opposite torque. Nonetheless, this numerical experiment is useful to understand the more complex wrapped

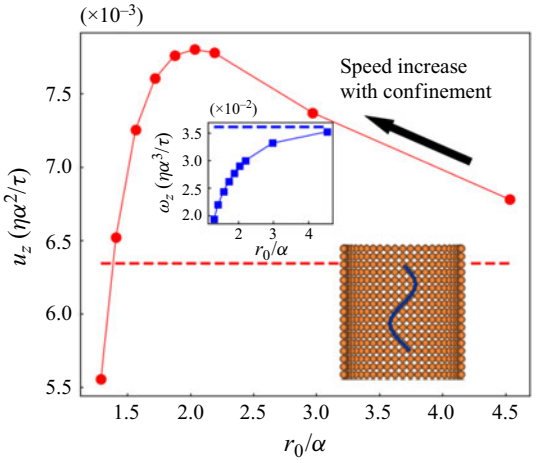

Figure 4. Swimming speed, u_z, and z-component of the angular velocity (inset), ω_z, of a single helical flagellum with amplitude $\alpha = 0.32$ μm (model II) inside a pipe of radius r_0. The dashed lines depicts the bulk values and a snapshot of the flagellum in a pipe is shown in the inset.

mode. We observe an increase in the swimming speed for decreasing pipe radius with respect to the bulk value above a critical pipe radius, see figure 4, similar to the wrapped mode results. For the single flagellum, its swimming speed can be written as $u_z = M_{tr}\tau_z$. For moderate confinements the hydrodynamic interactions with the wall increase the value of the mobility coupling term, M_{tr}, with respect to the bulk values, thus, the swimming speed is increased. For very tight confinements the lubrication interactions dominate the interactions with the wall and M_{tr} decreases below the bulk values. These effects were already reported by Liu, Breuer & Powers (2014) for an infinite flagellum within an infinite pipe. This speed increase is observed despite the reduction in the flagellum angular velocity, ω_z, with r_0, see figure 4 inset.

For the whole bacterium the situation is more complex because, at the same time that the flagellum thrust is enhanced, an additional drag on the bacterium body tends to reduce the swimming speed. This interplay between the enhanced thrust and the additional drag has been observed in a recent experimental study with *E. coli* (Vizsnyiczai *et al.* 2020). Vizsnyiczai *et al.* observed that a bacterium swimming in an extended mode inside a pipe swims slower than a bacterium in a channel. However, when the bacterium is exiting the pipe and only its flagellum remains inside, the swimming speed is larger than in a channel, showing the increased translation–rotational coupling experienced by the flagellum and the lack of an additional drag acting on the bacterium body (Vizsnyiczai *et al.* 2020). Our numerical results agree with the experimental work of Vizsnyiczai *et al.* for the extended mode while they suggest that, for the wrapped mode, the enhanced thrust is the dominant effect.

To explore in more detail the difference between the two swimming configurations we introduce a minimal model in which we treat the bacterium body and flagellum as two connected rigid bodies that move exactly along the pipe axis and are free to rotate along their axes (Vizsnyiczai *et al.* 2020). Thus, in the minimal model the velocities perpendicular to the pipe axis are assumed to be zero, unlike in the previous simulations. Taking into account that the bacterium is a free-force-torque swimmer we can write the

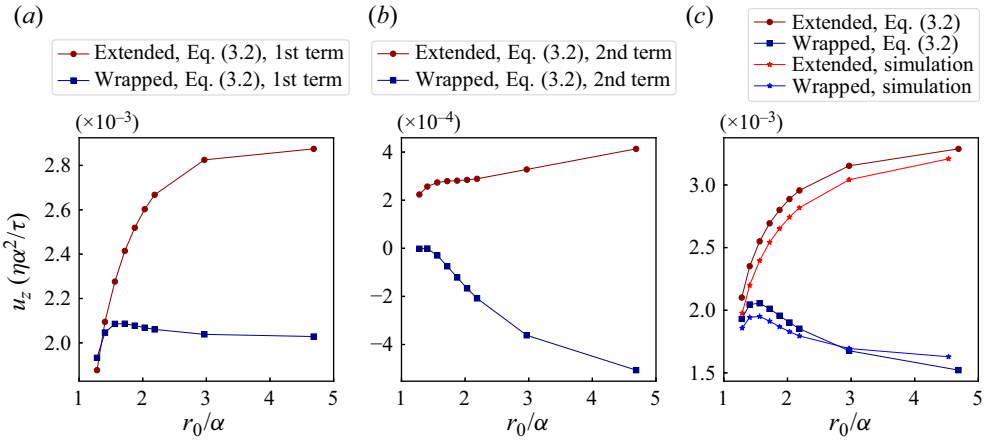

Figure 5. Swimming velocity normalized by the motor torque predicted by the first and second terms of the minimal model, (3.2), panels (*a*,*b*), respectively, and the full (3.2) compared with the hydrodynamic simulations, panel (*c*).

linear system

$$\begin{bmatrix} u_z \\ \omega_z^{body} \\ u_z \\ \omega_z^{flag} \end{bmatrix} = \begin{bmatrix} M_{tt} & 0 & C_{tt} & C_{tr} \\ 0 & M_{rr} & C_{rt} & C_{rr} \\ C_{tt} & C_{rt} & N_{tt} & N_{tr} \\ C_{tr} & C_{rr} & N_{tr} & N_{rr} \end{bmatrix} \begin{bmatrix} f_z \\ \tau_z \\ -f_z \\ -\tau_z \end{bmatrix}. \tag{3.1}$$

All the mobility components in (3.1) depend on the pipe radius and the bacterium mode (extended or wrapped) due to the hydrodynamic interactions. The unknowns in the linear system are the swimming velocity, u_z, the angular velocities of body and flagellum, ω_z^{body} and ω_z^{flag}, and the force acting on each of them f_z. Solving these equations for the swimming velocity we obtain

$$u_z = -\frac{(M_{tt} - C_{tt})\,(N_{tr} - C_{rt})}{M_{tt} + N_{tt} - 2C_{tt}}\tau_z + \frac{(N_{tt} - C_{tt})\,C_{tr}}{M_{tt} + N_{tt} - 2C_{tt}}\tau_z. \tag{3.2}$$

We compute numerically all the mobility components and plot the contribution of the first and second terms of (3.2) in figure 5. Panel (*a*) shows that the first term in (3.2) is the dominant one. It also shows that the decay in the speed is more pronounced for the extended mode, which occurs due to a stronger decay of M_{tt} and N_{tr} due to the hydrodynamic drag generated by the pipe. The contribution of the second term of (3.2) is qualitatively different for both modes, as shown in figure 5(*b*). The mobility component C_{tr} decays to almost zero for the wrapped mode but not for the extended mode. For the wrapped mode that term was a negative contribution, thus, when it vanishes it leads to an overall speed increase. The minimal model, including both the first and second terms of (3.2), explains the full numerical result reasonably well, as shown in figure 5(*c*). Thus, the main difference between the two swimming modes is a lower decrease of the coefficients M_{tt} and N_{tr} in the wrapped mode.

To further understand the difference between the two swimming modes we compute the flow around the bacterium in a tight pipe, with $r_0/\alpha = 1.56$, using the highest resolution model, with ∼16 times the number of blobs than the original simulations, see the Appendix. For the extended mode we show the instantaneous and the average flow field during one flagellum rotation in figure 6(*a*,*b*). The same flows for the wrapped mode

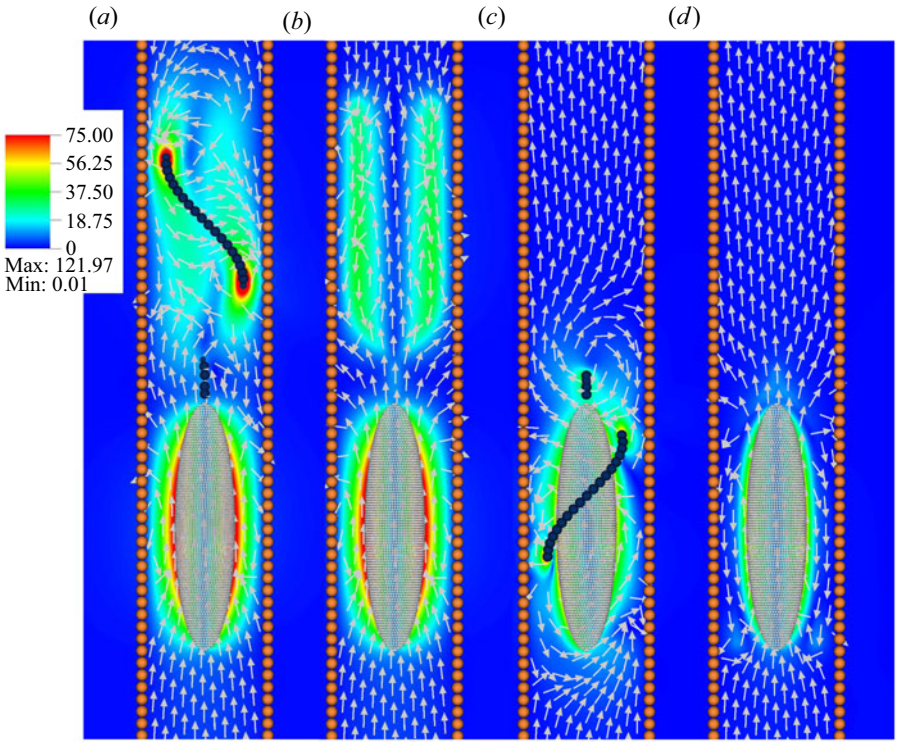

Figure 6. In-plane velocity fields around a bacterium inside a pipe with inner radius $r_0/\alpha = 1.56$. Instantaneous and average flow fields during one flagellum rotation for the extended mode, (*a*,*b*), respectively, and for the wrapped mode (*c*,*d*). The flagellum is not shown in the panels with the average flows (*b*,*d*). See also supplementary movie 1 available at https://doi.org/10.1017/jfm.2024.594.

are shown in figure 6(*c*,*d*). As the bacterium moves along the pipe an equivalent volume of fluid is displaced to make room for the bacterium, after all, the fluid is incompressible. The fluid can be pushed further along the pipe or transported to the back of the bacterium but, interestingly, flow perturbations decay exponentially fast along the pipe (Liron & Shahar 1978), therefore, it follows that, in long enough pipes, all the fluid displaced would be moved to the back of the bacterium. We can see in figure 6(*b*) a counter-flow close to the pipe wall. However, the high velocity gradients suggest a large drag that we observed as a reduction in the bacterium swimming speed. In the wrapped mode the flagellum works as an Archimedes' screw, helping to push fluid to the back of the bacterium, see figure 6(*d*). The effect of the flagellum pushing the fluid is observed more clearly in supplementary movie 1. This is the ultimate mechanism that differentiates the two swimming modes and makes the additional drag on the body the dominant effect for the extended mode and the enhanced rotation–translation coupling the dominant one for the wrapped mode.

3.1. *Power and efficiency*

The power consumption is an important quantity for a microswimmer propelling in a viscous environment and the efficiency can be more important than the absolute swimming speed. Thus, we measure these quantities. Considering that the chemical energy used within the cell is beyond the scope of our work, we limit ourselves to studying the power dissipated by the Stokes flow and the microswimmers hydrodynamic efficiency. The power

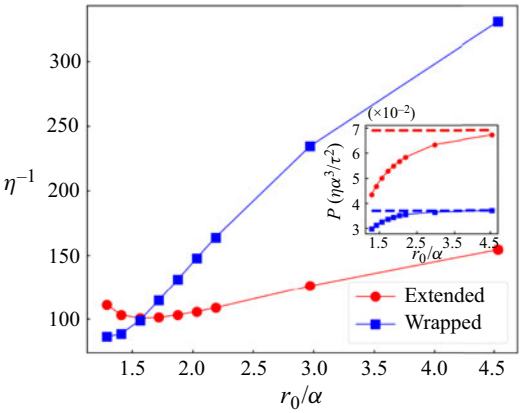

Figure 7. Inverse of the efficiency vs radius of the pipe (r_0). The inset shows the swimming power and the dashed lines depict the bulk values.

exerted by a microswimmer on the medium and dissipated by the flow is

$$P = \sum_n \left(\boldsymbol{f}_n \cdot \boldsymbol{u}_n + \boldsymbol{\tau}_n \cdot \boldsymbol{\omega}_n \right), \tag{3.3}$$

where the sum is over rigid bodies, in our case the bacterium body and its flagellum. As the power is generated by the motor, the power consumed by a bacterium during its swimming can be rewritten as $P_m = \boldsymbol{\tau}_m \cdot \boldsymbol{\omega}_m = \boldsymbol{\tau}_m \cdot (\boldsymbol{\omega}_{flag} - \boldsymbol{\omega}_{body})$. In the absence of elastic or soft steric interactions the two expressions are equivalent. We will always use (3.3) to account for the soft steric interactions used in § 3.3.

The wrapped mode consumes less power for all pipe radii owing to the slower rotation of its flagellum, see figure 7 inset. Under confinement the power exerted by the motor decays for both swimming modes. Of more interest is the hydrodynamic efficiency of the swimmers in propelling themselves. There are several approaches to defining the hydrodynamic efficiency (Childress 2012). We follow a classical approach and define the inverse efficiency as the power normalized with the power necessary to pull the bacterium body with the same speed (Higdon 1979; Lauga & Eloy 2013)

$$\eta^{-1} = \frac{M_{zz}}{u_z^2} P, \tag{3.4}$$

where $M_{zz} = u_z/f_z$ is body mobility (without flagellum) along the pipe axis and u_z the velocity. Figure 7 shows the inverse efficiency as a function of the pipe radius. In bulk and wide pipes the extended mode is more efficient. However, there is a cross-over and for tight confinements the wrapped mode becomes more efficient. This is a result of the lower power consumption of the wrapped mode and, importantly, its enhanced velocity within the pipe. This result suggests that the wrapped mode has an advantage for propulsion in confined spaces. To verify the accuracy of the results we perform a resolution study by increasing the resolution by factors of 4 and 16 and we obtain essentially the same results as shown in the Appendix and figure 10. So far we have only used one flagellum, model II, and a bacterium placed exactly on the middle of the pipe. In the next two sections we explore whether these results are robust under a change in these conditions.

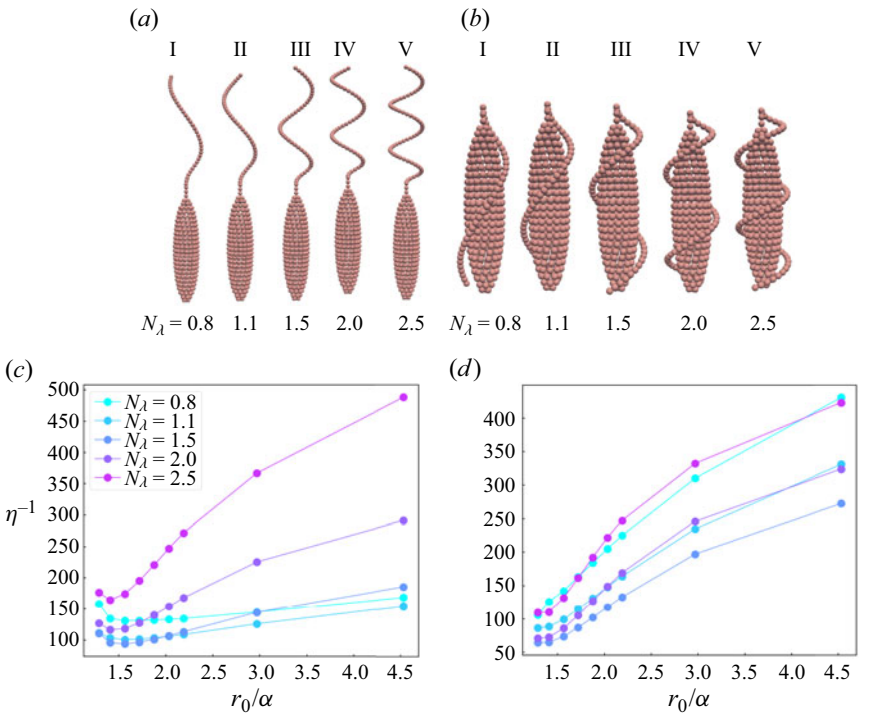

Figure 8. Shapes of extended (*a*) and wrapped (*b*) bacterium modes with different N_λ values. Inverse of the swimming efficiency vs radius of the pipe (r_0) for different values of N_λ for the extended mode (*c*) and the wrapped mode (*d*).

3.2. *Robustness of results: effect of N_λ and L*

Bacterial species present flagella of different lengths, amplitudes and pitch angles which affect the bacterium bulk speeds and efficiencies (Higdon 1979; Lauga & Eloy 2013). Here, we explore if the wrapped mode is a more efficient swimming style in confined environments for a wide variety of flagellum models. We build five flagellum models by varying simultaneously the flagellum length, L, and the number of waves along its length, $N_\lambda = L_z/\lambda$, where L_z is the flagellum extension along its axis and λ the wavelength of the helical wave, see figure 8(*a*,*b*) and table 1. We present the inverse efficiency for all flagellum models and pipe radii in figure 8(*c*,*d*).

The general trend is the same as before. For wide pipes the extended mode is more efficient than the wrapped mode for all flagellum models except one ($N_\lambda = 2.5$). Under confinement both swimmers increase their efficiency but the improvement is stronger for the wrapped mode, which becomes the most efficient for pipes with $r_0/\alpha \lessapprox 1.7$. In those situations the wrapped mode is approximately two times more efficient than the extended mode. The efficiency, for both swimming modes, is non-monotonic in N_λ. When $N_\lambda \ll 1$ the flagellum is almost straight, thus, it cannot propel the bacterium. Therefore, the swimming speed and the efficiency initially grow with N_λ. Beyond a certain value of N_λ the flagellum tangent forms a large angle with the direction of motion, which again reduces the propulsion efficiency. For intermediate values of N_λ the flagellum is helical shaped, which allows propulsion. For both modes the flagellum with $N_\lambda = 1.5$ is the most efficient under confinement for the flagellum lengths considered. For bacteria swimming in bulk the optimum is also close to $N_\lambda = 1.5$, although the exact optimum N_λ depends

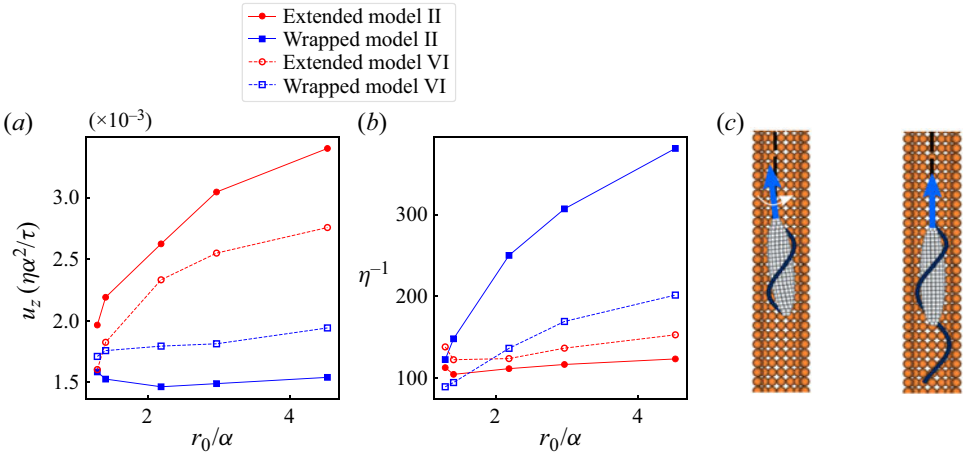

Figure 9. Swimming speed (*a*) and hydrodynamic efficiency (*b*) of wrapped and extended modes swimming along a periodic pipe extracted from 10 s long dynamic simulations. Full symbols use flagellum model II, which extends the same length as the body, and open symbols use model flagellum VI, which extends longer. The longer flagellum prevents the tilt of the wrapped mode, which results in higher speeds and better efficiencies. (*c*) Two bacteria inside a pipe. A bacterium with a short flagellum performs a precession motion around the pipe axis while a bacterium with a long flagellum is forced to swim straight. The swimming direction is shown with a large arrow and the pipe axis with a dashed line.

on the flagellum length (Higdon 1979). For the extended mode, optimal swimming occurs around the non-dimensional pipe radius, $r_0/\alpha = 1.5$ for all values of N_λ. For the wrapped mode the optimal swimming occurs for lower values of r_0/α.

3.3. *Robustness of results: dynamical simulations*

So far we have computed the swimming speed when the bacterium is located in the middle of the pipe and aligned along it. However, freely swimming bacteria can tilt and move towards the pipe wall. To verify if the results reported so far are robust, we perform dynamic simulations where the bacterium is free to displace away from the pipe centreline and to change orientations. We use the same pipe models as before but impose periodic boundary conditions along the pipe. To solve the Stokes equations with these boundary conditions we use a periodic fast multipole method implemented in the library STKFMM (Yan & Shelley 2018). To avoid the overlap of the bacterium with the pipe we include a steric repulsion interaction between the blobs of pipe and bacterium with a repulsion strength of $f = 0.05$ pN for overlapping blobs and with an exponential decay with a characteristic length $\xi = 0.01$ μm for non-overlapping blobs. As in § 2.1 we use a midpoint integrator to integrate the equations of motion (Balboa Usabiaga & Delmotte 2022). In all simulations we use the same time step size, $\Delta t = 10^{-3}$s, so a full flagellum rotation takes around 12 (36) time steps for the fastest (slowest) rotating flagella. For all models considered in this section we simulate the bacterium for 10 s so the bacterium can swim at least 70 μm. We use the last 8 s to extract the swimming speed and the power consumption.

We observe that the bacterium swimming in the extended mode swims near the pipe walls while bacterium swimming in the wrapped mode tries to remain away from them. This lateral displacement is more evident in wide pipes where the bacterium has more space to move, see supplementary movie 2, and it is reminiscent of the hydrodynamic attraction to walls by the extended mode mentioned in § 2.1 and the hydrodynamic

repulsion from walls experienced by the wrapped mode (not shown). The swimming speed and efficiency, for the bacterium with flagellum model II, are shown in figure 9. The same general trend as for the static simulations is observed. However, the efficiency curves do not cross-over. The cross-over is not observed because this time the wrapped swimming speed along the pipe, u_z, barely increases with confinement, and the efficiency depends strongly on u_z. The magnitude of u_z does not increase because the bacterium swims with a tilt towards the wall, see figure 9(*c*) and supplementary movie 3. In contrast, the extended mode cannot tilt significantly in small pipes as that is prevented by its rigid flagellum, which favours the motion along the pipe.

To verify if the whole extension of the swimmers affects the result we run another set of simulations using a longer flagellum, model VI, that extends beyond the bacterium body, see figure 9(*c*) and supplementary movie 4. The results are presented as open symbols in figure 9. In this case the speed of the wrapped mode is approximately independent on the confinement but larger than with the shorter flagellum. As a result we observe a cross-over between the efficiencies of the wrapped and extended modes. Overall, these results show that (i) the swimming speed is less sensitive to confinement for the wrapped mode than for the extended mode, (ii), the efficiency improves strongly for the wrapped mode and (iii), depending on the flagellum details, the wrapped mode can be the most efficient way to swim under confinement.

4. Conclusions

In this paper we have presented the dynamics of two different swimming modes, namely the extended and wrapped modes of monotrichous-type bacteria. Under bulk conditions the extended mode swims faster and more efficiently than the wrapped mode. However, under strong confinement the efficiency of the wrapped mode improves faster than for the extended mode. For a wide number of flagellum shapes, with different lengths and wavelengths, the bacterium in the wrapped mode swims more efficiently. For both swimming modes the flagellum rotation–translation coupling is enhanced by the pipe confinement (Liu *et al.* 2014; Vizsnyiczai *et al.* 2020). However, the drag on the bacterium body is also increased and only for the wrapped mode is the enhanced flagellum coupling the dominant effect. The flow fields around the bacterium suggest that the wrapped mode works as an Archimedes' screw helping to transport the fluid displaced by the motion of the bacterium. Such a screw-like configuration improves the swimming efficiency.

These results are complementary to the experimental work of Kinosita *et al.* where the bacterium *Burkholderia* adopting the wrapped mode was observed to glide in very narrow ducts (Kinosita *et al.* 2018). It seems that, either by gliding over a substrate or by means of hydrodynamic interactions, the wrapped mode promotes the motion of bacteria in tight confinements. It is interesting to note that some bipolar flagellated bacteria can display a wrapped and an extended mode simultaneously, where the flagellum at the front pole wraps around the body and the rear one remains extended (Murat *et al.* 2015; Constantino *et al.* 2018; Thormann *et al.* 2022; Bansil *et al.* 2023). Such a mixed mode could present some advantages under confinement that should be investigated.

Supplementary movies. Supplementary movies are available at https://doi.org/10.1017/jfm.2024.594.

Funding. The project that gave rise to these results received the support of a fellowship from 'la Caixa' Foundation (ID 100010434), fellowship LCF/BQ/PI20/11760014 and from the European Union's Horizon 2020 research and innovation programme under the Marie Skłodowska-Curie grant agreement no. 847648. Funding provided by the Basque Government through the BERC 2022-2025 program and by the Ministry of Science and Innovation: BCAM Severo Ochoa accreditation CEX2021-001142-S/MICIN/AEI/10.13039/501100011033

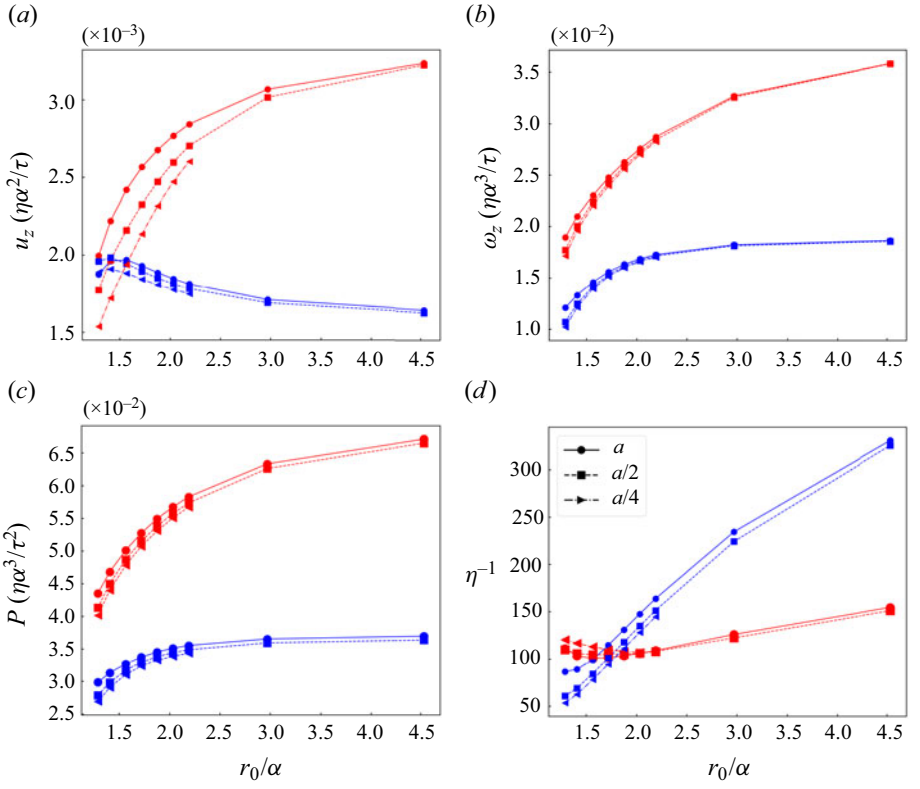

Figure 10. (*a*) Swimming speed, (*b*) flagellum angular speed, (*c*) swimming power and (*d*) inverse of the efficiency vs pipe radius for three different resolutions with blob radii a, $a/2$ and $a/4$. Red curve symbols extended mode and blue curve symbols wrapped mode.

and the project PID2020-117080RB-C55 'Microscopic foundations of soft matter experiments: computational nano-hydrodynamics (Compu-Nano-Hydro)' is also acknowledged.

Declaration of interests. The authors report no conflict of interest.

Author ORCIDs.
H. Gidituri https://orcid.org/0000-0001-6552-9587;
M. Ellero https://orcid.org/0000-0001-8894-0395;
F. Balboa Usabiaga https://orcid.org/0000-0003-0130-3532.

Appendix. Resolution study

Here, we conduct a resolution study to verify the robustness of our results. We reduce the blob radius used to discretize the bacterium body and the pipes from a to $a/2$ and $a/4$ while at the same time increasing the resolution so the numbers of blobs are $\sim$4 and $\sim$16 larger than in the original model, respectively. We do not refine the flagellum as its thickness, proportional to the blob radius, should remain constant during the resolution study.

For these three resolutions we measure the swimming speed (u_z), flagellum rotational speed (ω_z), swimming power (P) and inverse efficiency (η^{-1}). The results are presented in figure 10. There are some differences in the swimming speed, see figure 10(*a*). However, the other quantities only show a small deviation with respect to the original resolution.

The cross-over in the inverse of the efficiency between the wrapped and the extended mode is more pronounced for the highest resolution considered, see figure 10(*d*). More important, the overall trends observed for all the magnitudes measured remain unchanged for all resolutions, and thus, the results are robust against the resolution of the model.

References

Balboa Usabiaga, F. & Delmotte, B. 2022 A numerical method for suspensions of articulated bodies in viscous flows. *J. Comput. Phys.* **464**, 111365.

Balboa Usabiaga, F., Kallemov, B., Delmotte, B., Bhalla, A.P.S., Griffith, B.E. & Donev, A. 2016 Hydrodynamics of suspensions of passive and active rigid particles: a rigid multiblob approach. *Commun. Appl. Maths Comput. Sci.* **11** (2), 217–296.

Bansil, R., Constantino, M.A., Su-Arcaro, C., Liao, W., Shen, Z. & Fox, J.G. 2023 Motility of different gastric helicobacter spp. *Microorganisms* **11** (3), 634–648.

Childress, S. 2012 A thermodynamic efficiency for Stokesian swimming. *J. Fluid Mech.* **705**, 77–97.

Constantino, M.A., Jabbarzadeh, M., Fu, H.C., Shen, Z., Fox, J.G., Haesebrouck, F., Linden, S.K. & Bansil, R. 2018 Bipolar lophotrichous helicobacter suis combine extended and wrapped flagella bundles to exhibit multiple modes of motility. *Sci. Rep.* **8** (1), 1–15.

Das, D. & Lauga, E. 2018 Computing the motor torque of *Escherichia coli*. *Soft Matt.* **14**, 5955–5967.

Grognot, M. & Taute, K.M. 2021 More than propellers: how flagella shape bacterial motility behaviors. *Curr. Opin. Microbiol.* **61**, 73–81.

Higdon, J.J.L. 1979 The hydrodynamics of flagellar propulsion: helical waves. *J. Fluid Mech.* **94** (2), 331–351.

Kinosita, Y., Kikuchi, Y., Mikami, N., Nakane, D. & Nishizaka, T. 2018 Unforeseen swimming and gliding mode of an insect gut symbiont, Burkholderia sp. RPE64, with wrapping of the flagella around its cell body. *ISME J.* **12** (3), 838–848.

Kühn, M.J., Schmidt, F.K., Eckhardt, B. & Thormann, K.M. 2017 Bacteria exploit a polymorphic instability of the flagellar filament to escape from traps. *Proc. Natl Acad. Sci. USA* **114** (24), 6340–6345.

Kühn, M.J., Schmidt, F.K., Farthing, N.E., Rossmann, F.M., Helm, B., Wilson, L.G., Eckhardt, B. & Thormann, K.M. 2018 Spatial arrangement of several flagellins within bacterial flagella improves motility in different environments. *Nat. Commun.* **9** (1), 5369.

Lauga, E., DiLuzio, W.R., Whitesides, G.M. & Stone, H.A. 2006 Swimming in circles: motion of bacteria near solid boundaries. *Biophys. J.* **90** (2), 400–412.

Lauga, E. & Eloy, C. 2013 Shape of optimal active flagella. *J. Fluid Mech.* **730**, R1.

Liron, N. & Shahar, R. 1978 Stokes flow due to a Stokeslet in a pipe. *J. Fluid Mech.* **86** (4), 727–744.

Liu, B., Breuer, K.S. & Powers, T.R. 2014 Propulsion by a helical flagellum in a capillary tube. *Phys. Fluids* **26** (1), 011701.

Murat, D., Hérisse, M., Espinosa, L., Bossa, A., Alberto, F. & Wu, L.-F. 2015 Opposite and coordinated rotation of amphitrichous flagella governs oriented swimming and reversals in a magnetotactic spirillum. *J. Bacteriol.* **197** (20), 3275–3282.

Park, J., Kim, Y., Lee, W. & Lim, S. 2022 Modeling of lophotrichous bacteria reveals key factors for swimming reorientation. *Sci. Rep.* **12** (1), 6482.

Pimponi, D., Chinappi, M., Gualtieri, P. & Casciola, C.M. 2016 Hydrodynamics of flagellated microswimmers near free-slip interfaces. *J. Fluid Mech.* **789**, 514–533.

Shum, H., Gaffney, E.A. & Smith, D.J. 2010 Modelling bacterial behaviour close to a no-slip plane boundary: the influence of bacterial geometry. *Proc. R. Soc. Lond.* A **466** (2118), 1725–1748.

Thormann, K.M., Beta, C. & Kühn, M.J. 2022 Wrapped up: the motility of polarly flagellated bacteria. *Annu. Rev. Microbiol.* **76** (1), 349–367.

Tian, M., Wu, Z., Zhang, R. & Yuan, J. 2022 A new mode of swimming in singly flagellated pseudomonas aeruginosa. *Proc. Natl Acad. Sci. USA* **119** (14), e2120508119.

Vizsnyiczai, G., Frangipane, G., Bianchi, S., Saglimbeni, F., Dell'Arciprete, D. & Di Leonardo, R. 2020 A transition to stable one-dimensional swimming enhances *E. coli* motility through narrow channels. *Nat. Commun.* **11** (1), 2340.

Wajnryb, E., Mizerski, K.A., Zuk, P.J. & Szymczak, P. 2013 Generalization of the Rotne–Prager–Yamakawa mobility and shear disturbance tensors. *J. Fluid Mech.* **731**, R3.

Xing, J., Bai, F., Berry, R. & Oster, G. 2006 Torque–speed relationship of the bacterial flagellar motor. *Proc. Natl Acad. Sci. USA* **103** (5), 1260–1265.

Yan, W. & Shelley, M. 2018 Universal image system for non-periodic and periodic Stokes flows above a no-slip wall. *J. Comput. Phys.* **375**, 263–270.